Front. Earth Sci. 2025, 19(2): 246–260
https://doi.org/10.1007/s11707-024-1136-8

RESEARCH ARTICLE

Interannual variability and trends of gross primary production and transpiration in savannas and grasslands from 2000 to 2021

Cheng MENG[1], Xiangming XIAO (✉)[1], Li PAN[1], Baihong PAN[1], Russell L. SCOTT[2], Pradeep WAGLE[3], Chenchen ZHANG[1], Yuan YAO[1], Yuanwei QIN[1]

1 School of Biological Sciences, Center for Earth Observation and Modeling, University of Oklahoma, Norman OK 73019, USA
2 Southwest Watershed Research Center, USDA Agricultural Research Service, Tucson AZ 85719, USA
3 Oklahoma and Central Plains Agricultural Research Center, USDA Agricultural Research Service, EI Reno OK 73036, USA

Abstract Carbon and water fluxes of savannas and grasslands have large seasonal dynamics and inter-annual variation. In this study, we selected five savanna and grassland sites, each of them having 10+ years (11–21 years) of eddy covariance (EC) data, and a total of 85 site-years at these five sites which offers a unique opportunity for data analyses and model evaluation. We ran a long-term simulation (2000–2021) of the vegetation photosynthesis model (VPM, v3.0) and vegetation transpiration model (VTM, v2.0) to investigate the seasonal dynamics, interannual variation, and decadal trends of modeled gross primary production (GPP_{VPM}) and transpiration (T_{VTM}) at these sites. The seasonal dynamics of daily GPP_{VPM} and T_{VTM} track well with the seasonal dynamics of EC-based GPP (GPP_{EC}, R^2: 0.76–0.93) and evapotranspiration (ET_{EC}, R^2: 0.69–0.92). The inter-annual variation of annual GPP_{VPM} tracked well that of annual GPP_{EC}, with the linear regression slopes for GPP_{EC} versus GPP_{VPM-EC} ranging from 0.89 to 1.11. The simulation results of GPP_{VPM} and T_{VTM} using two different climate data sets (*in situ* climate data and European Center for Medium-Range Weather Forecasts Reanalysis v5 data set (ERA5)) were similar, suggesting that ERA5 data can be used for VPM/VTM simulations at large spatial scales. From 2000 to 2021, annual GPP_{VPM} and T_{VTM} had no significant inter-annual trends at one savanna and three grassland sites but increased significantly at one savanna site. The results demonstrate the potential of using VPM (v3.0) and VTM (v2.0) to predict the seasonal dynamics and inter-annual variation of GPP and T in savannas and grasslands.

Received April 15, 2024; accepted September 30, 2024

E-mail: xiangming.xiao@ou.edu

Keywords vegetation photosynthesis model, vegetation transpiration model, ERA5, MODIS, carbon fluxes

1 Introduction

Savannas and grasslands together account for nearly 50% of the earth's land surface and are critical for terrestrial carbon cycles and ecosystem services (O'Mara, 2012; Kemp et al., 2013). They contribute the most to the interannual variation of terrestrial carbon sinks or sources, accounting for 51% of the variability (Biederman et al., 2017). Carbon cycles in grasslands and savannas are sensitive to air temperature and precipitation (Peng et al., 2013; Wagle et al., 2015a). The large variability in both timing and amount of precipitation in these areas leads to large inter-annual variability in gross primary production (GPP), making it difficult to estimate GPP in these areas. For example, one of the most widely used global GPP products (MOD17A2) underestimated GPP by 34% in 15 grassland sites with multi-year observations (> 5 years) around the world (Zhu et al., 2018). Another study found that some satellite-based models captured only 40% to 53% interannual variability of GPP at a woody savanna site (Scott et al., 2023). The under-estimation from these models can be attributed to underestimated values of the maximum light use efficiency parameter, uncertainty in estimating the fraction of absorbed photosynthetically active radiation (FPAR), and the uncertainty in estimating the effect of water stress on GPP (Sjöström et al., 2013; Zhu et al., 2018). Evapotranspiration (ET) comprises both soil and vegetation evaporation (E) and vegetation transpiration (T), playing a vital role in linking terrestrial water,

carbon, and surface energy exchanges (Gentine et al., 2019). The projected changes in precipitation from future climate change scenarios may result in changes in plant water availability and GPP, making it more difficult to estimate spatial-temporal patterns of carbon and water fluxes (Swain et al., 2018; Konapala et al., 2020). Therefore, accurate observation and modeling of carbon and water cycles in these regions are needed.

The eddy covariance (EC) technique provides a continuous and reliable measurement of carbon dioxide (CO_2) and water vapor (H_2O) fluxes (Baldocchi, 2014). The GPP derived from EC sites (GPP_{EC}) has been widely used to support the development of process-based models and satellite-based remote sensing models (Jiang and Ryu, 2016; Zhang et al., 2017; Zheng et al., 2020). However, partitioning ET measured by EC instrumentation (ET_{EC}) into evaporation (E) and transpiration (T) is less common, limiting the development of process-based models to estimate T (Stoy et al., 2019). Several EC data-based techniques have been developed to partition ET, including the partition models that used the relationship between GPP and ET (Zhou et al., 2016; Scott and Biederman, 2017; Nelson et al., 2020), and the models that estimated canopy and soil conductance (Li et al., 2019). However, these models are dependent on the GPP_{EC} over the EC tower sites with varying sizes and shapes of footprints ranging from several hundred meters to kilometers.

Satellite remote sensing provides another option for estimating CO_2 and H_2O fluxes. Several light-use efficiency (LUE)-based production efficiency models (PEMs) have been developed to estimate the GPP of terrestrial ecosystems, driven by vegetation indices derived from optical images and climate data (Goetz et al., 1999; Turner et al., 2003; Zhao et al., 2005; Zhang et al., 2017; Zheng et al., 2020). As one of the LUE-based PEMs, the Vegetation Photosynthesis Model (VPM) uses the concept of light absorption by chlorophyll ($APAR_{chl}$) and considers the effect of air temperature (T_{scalar}) and water (W_{scalar}) stresses on LUE (Xiao et al., 2004a, 2024b). The biome-specific optimum air temperature parameter ($TA_{opt\text{-}biome}$) values were used in VPM v2.0 for savannas and grasslands (Zhang et al., 2017). A recent study introduced a site-specific TA_{opt} ($TA_{opt\text{-}site}$) parameter and assessed its effect on GPP estimation over 11 grassland sites (Chang et al., 2020). In addition, the vegetation transpiration model (VTM, v1.0) was developed to estimate T based on the intrinsic interactions between CO_2 (photosynthesis) and water (transpiration) processes at the leaf level and was evaluated with one-year data from 10 grassland sites in the US Southern Great Plains, as part of the 2002 International H_2O project (Alfieri et al., 2009). VTM estimates transpiration (T_{VTM}) as a function of GPP and transpiration ratio that is an inverse of water use efficiency (WUE). The GPP data used in VTM can come from either eddy flux tower sites (GPP_{EC}) or the VPM model (GPP_{VPM}).

In this study, we selected five savanna and grassland sites, each of which has 10+ (11−21 years) years of continuous EC measurements and ran VPM and VTM at these five sites with MODIS images and ERA5 climate data from 2000 to 2021. The objectives were to: i) understand the seasonal dynamics, inter-annual variation, and decadal change of climate, vegetation indices (Normalized Difference Vegetation Index (NDVI), Enhanced Vegetation Index (EVI), Land Surface Water Index (LSWI)), and carbon and water fluxes at these sites; ii) assess the performance of VPM v3.0 and VTM v2.0 to predict seasonal dynamics and interannual variation of GPP and T; iii) investigate inter-annual variation and decadal change (trend) of atmospheric CO_2 concentration, climate, vegetation indices (NDVI, EVI, LSWI), GPP, and T from 2000 to 2021. The two research questions we asked are: i) can the VPM v3.0 and VTM v2.0 well simulate the seasonal dynamics and interannual variation of GPP and T in these grassland and savanna sites over the last two decades; ii) what are the inter-annual variation and trend of atmospheric CO_2 concentration, climate, vegetation indices (NDVI, EVI, LSWI), GPP, and T in these grassland and savanna sites over the last two decades. This site-level study with 10+ years of *in situ* data and VPM and VTM model simulations over the two decades will improve our understanding of carbon and water fluxes in savannas and grasslands and provide a case study that would help us to carry out regional and global simulations in the near future.

2 Materials and methods

2.1 Study sites

In this study, we selected two savanna sites (US-TON and US-SRM) and three grassland sites (US-VAR, US-SRG, and US-WKG). Among the grassland and savanna sites in the AmeriFlux network, these five sites have 10+ years of continuous measurements and the data that are available to the public range from 11 to 21 years (Table 1). The geo-locations of the five sites are shown in Fig. 1(a). Landscape features of the five sites are shown in Fig. 1. A summary of vegetation composition and climate characteristics of the five sites are listed in Table 1. Detailed descriptions of the five sites can be found on the AmeriFlux website.

2.2 Data sources

2.2.1 *In situ* data at the eddy flux tower sites

All CO_2, H_2O, energy, and meteorological data were downloaded from the AmeriFlux (US-VAR, US-TON,

Table 1 Summary of geographical location, climate, soil, and vegetation at the five study sites

Site name	US-VAR	US-TON	US-WKG	US-SRG	US-SRM
Data availability in AmeriFlux/ Fluxnet2015	2000–2021	2001–2021	2004–2021	2008–2021	2004–2014
Latitude (°)	38.4133	38.4309	31.7365	31.7894	31.8214
Longitude (°)	−120.9508	−120.9660	−109.9419	−110.8277	−110.8661
Elevation (m)	129	177	1531	1291	1120
MAT (°C)	15.1	15.8	15.6	17	17.9
MAP (mm)	559	559	407	420	380
Soil type	Silt loam	Silt loam	Loam	Sandy loam	Sandy loam
IGBP	GRA	WSA	GRA	GRA	WSA
Tree/ Shrub	Oak (*Quercus douglasii*)	Oak (*Quercus douglasii*)	*Calliadra eriophylla* and *Daleaformosam*	Mesquite (*Prosopis velutina*)	Mesquite (*Prosopis velutina*)
Grass	C3 grasses (*Erodium cicutarium*, *Hypochaeris glabra*, *Trifolium dubium* Sibth., *Trifolium hirtum* All., *Dichelostemma volubile* A., and *Erodium botrys* Cav.)	C3 grasses (*Brachypodium distachyon*, *Hypochaeris glabra*, *Trifolium hirtum*)	C4 grasses (*Bouteloua eriopoda*, *Bouteloua curtipendula*, *E.legmannana*)	C4 grasses (*Eragrostis lehmanniana*)	C4 grasses (*Digitaria californica*, *Muhlenbergia porteri*, *Bouteloua eriopoda*, *Aristida* spp., *Eragrostis lehmanniana*)
Tree/shrub cover	< 10%	~ 40%	~5%	~ 10%	~ 35%
C3/C4	100% / 0	100% / 0	10% / 90%	20% / 80%	40% / 60%
LAI	0.1–0.94	0.84–1.62	0.1–0.84	0.2–1.07	0.19–0.84
Reference	Xu and Baldocchi, (2004)	Ma et al., (2016)	Scott et al., (2015)	Scott et al., (2015)	Scott et al., (2015)

Notes: IGBP: International Geosphere–Biosphere Programme land cover classification; WSA: woody savanna, GRA: grassland; MAT: mean annual temperature; MAP: mean annual precipitation; C3/C4: the ratio of C3 plant and C4 plant; LAI: leaf area index.

US-WKG, and US-SRG) and FLUXNET2015 (US-SRM) website. The data sets consist of data at five temporal resolutions: half-hourly, daily, weekly, monthly, and yearly. Data were processed using a consistent and uniform processing pipeline (Pastorello et al., 2020). Half-hourly flux and meteorological data, including GPP_{EC}, latent heat flux (LE), photosynthetically active radiation (PAR_{EC}), air temperature, atmospheric CO_2 concentration, precipitation (P_{EC}), and soil water content (SWC_{EC}) were used in this study. The LE was used to calculate ET_{EC}. We used a threshold of incoming photosynthetic photon flux density greater than 0.5 μmol Photon·m^{-2}·s^{-1} to define the daytime period. Daily daytime mean air temperature ($TA_{DT\text{-}EC}$) was computed to drive VPM. Daily data were further averaged over an 8-day interval to match the temporal resolution of the MODIS 8-day composite images.

2.2.2 MODIS product during 2000–2021

Time-series MOD09A1 data (500-m spatial resolution and 8-day temporal resolution) for each site were extracted from the Google Earth Engine (GEE) based on the geo-location information (latitude and longitude) of individual sites. The quality detection method of QA bands was used to identify and discard bad-quality data (i.e., cloud and cloud shadow observations). The resultant missing (gap) observations in the time series data were gap-filled by the linear interpolation gap-fill method over a 3- or 5- observation window (t−1, t, t + 1, or t−2, t−1, t, t + 1, t + 2) to generate continuous good-quality surface reflectance MOD09A1 data. For each MODIS 8-day surface reflectance observation, blue (459–479 nm), red (620–670 nm), near-infrared (NIR1, 841–876 nm), and shortwave infrared (SWIR1, 1628–1652 nm) bands were used to calculate three vegetation indices: NDVI (Tucker, 1979), EVI (Huete et al., 1997; Huete et al., 2002), and LSWI (Xiao et al., 2004a, b).

2.2.3 ECMWF reanalysis v5 climate data (ERA5)

The ERA5 data set provides hourly data for many atmospheric and surface variables with ~9 km spatial resolution. Hourly resolutions of the air temperature, downward shortwave radiation, and precipitation were used to compute daily daytime mean air temperature ($TA_{DT\text{-}ERA5}$), daily downward shortwave radiation flux, and precipitation (P_{ERA5}), respectively. In this study, we used a constant ratio of 0.45 to convert incident shortwave radiation into photosynthetically active radiation (PAR_{ERA5}) (Ryu et al., 2018) and 4.56 μmol·J^{-1} as the energy-quanta conversion factor (Dye, 2004). Daily data were averaged over an 8-day interval, following the temporal resolution of MODIS 8-day composite images.

The comparison between TA_{DT} and PAR data from ERA5 and EC sites was shown in Fig. S1. Two California sites (US-VAR and US-TON) showed small differences (1%–4%) in TA_{DT} and PAR between ERA5 and EC data sets, with TA_{DT} *RMSE* ranging from 0.93°C to 1.29°C and $R^2 > 0.99$, and PAR *RMSE* ranging from 2.77 to 3.45

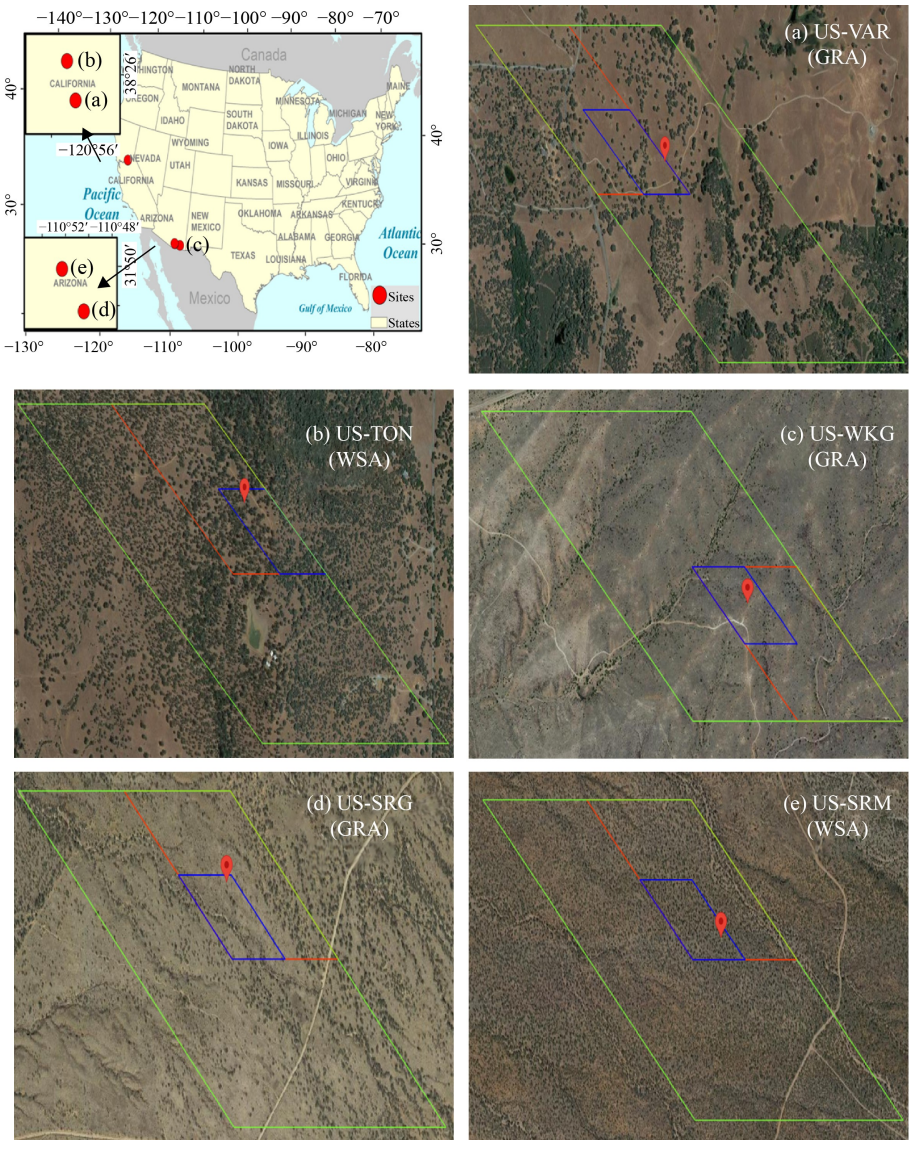

Fig. 1 The geolocation and landscape surrounding the locations of the five grassland and savanna EC tower sites in the USA (red dots) within a MODIS pixel at the 500 m spatial resolution (red box), the blue box indicated the 250 m spatial resolution, and the green box indicated the 1000 m spatial resolution. WSA: woody savanna, GRA: grassland.

and $R^2 > 0.99$. At the US-WKG site, $TA_{DT\text{-}ERA5}$ and PAR_{ERA5} were higher than $TA_{DT\text{-}EC}$ and PAR_{EC} (3% and 8% difference between 1:1 line). At the US-SRG site, $TA_{DT\text{-}ERA5}$ was 6% lower than $TA_{DT\text{-}EC}$ and PAR_{ERA5} was 11% higher than PAR_{EC}. At the US-SRM site, $TA_{DT\text{-}ERA5}$ was 7% lower than $TA_{DT\text{-}EC}$ and PAR_{ERA5} was 14% higher than PAR_{EC}. Thus, these results indicate the reanalysis data can be used with high confidence at the California sites. However, the reanalysis data should be used with caution for the sites in Arizona.

2.3 Models description and simulation

2.3.1 The Vegetation Photosynthesis Model (VPM v3.0)

The VPM was developed to estimate daily GPP (g $C \cdot m^{-2} \cdot day^{-1}$) as a product of light absorption by chlorophyll ($APAR_{chl}$) and light use efficiency (LUE, ε_g) (Xiao et al., 2004a, 2004; Xin et al., 2017; Chang et al., 2020). As shown in Eq. (1), The VPM estimates daily GPP as

$$GPP = APAR_{chl} \times \varepsilon_g, \quad (1)$$

where ε_g is the light use efficiency (μmol CO_2/μmol PPFD) and $APAR_{chl}$ is the amount of PAR absorbed by chlorophyll. $APAR_{chl}$ in Eq. (1) can be estimated as

$$APAR_{chl} = FPAR_{chl} \times PAR, \quad (2)$$

where PAR is the photosynthetically active radiation (μmol photosynthetic photon flux density, PPFD) and $FPAR_{chl}$ is the fraction of PAR absorbed by chlorophyll

in the canopy.

The $FPAR_{chl}$ is estimated as a linear function of EVI (Pan et al., 2024):

$$FPAR_{chl} = EVI - 0.1. \quad (3)$$

The coefficient of 0.1 is used to adjust for sparsely vegetated or barren land, which has been validated by solar-induced chlorophyll fluorescence data (Zhang et al., 2017).

The light use efficiency (ε_g) can be calculated as

$$\varepsilon_g = \varepsilon_0 \times T_{scalar} \times W_{scalar}, \quad (4)$$

where ε_0 is the maximum light use efficiency (g C/mol APAR), T_{scalar} and W_{scalar} are the downward regulation of temperature and water effects on maximum light use efficiency. The ε_0 is a fixed value acquired from literature and varies in C3 and C4 plants, with 0.53 g C·mol^{-1} APAR for C_3 plants, 0.79 g C·mol^{-1} APAR for C_4 plants, respectively (Xiao, 2006). In this study, we made educated guesses on C3/C4 plant ratios in each site based on plant cover estimates through communication with principal investigators at these sites (Table 1). For the two savanna sites (US-VAR and US-TON), there are no C4 grass plants, and the C3/C4 plant coverage ratio used in the model was 100%C3F and 0%C4F at the US-VAR site, 100%C3F and 0%C4F at the US-TON site. For the other three sites, the C3/C4 plant coverage ratios used in the model were 10%C3F and 90%C4F at the US-WKG site, 20%C3F and 80%C4F at the US-SRG site, 40%C3F and 60%C4F at the US-SRM site, respectively. So, in a pixel with different C_3 and C_4 plant fractions (C3F and C4F), ε_0 can be calculated as

$$\varepsilon_0 = C3F \times \varepsilon_{0-C3} + C4F \times \varepsilon_{0-C4}. \quad (5)$$

The T_{scalar} is calculated by the following equation:

$$T_{scalar} = \frac{(TA - TA_{max}) \times (TA - TA_{min})}{(TA - TA_{max}) \times (TA - TA_{min}) - (TA - TA_{opt})^2}, \quad (6)$$

where TA, TA_{max}, TA_{min}, and TA_{opt} are daily daytime mean air temperature, maximum, minimum, and optimum temperature for photosynthesis, respectively. When the air temperature falls below TA_{min}, TA_{scalar} is set to zero. TA_{max} and TA_{min} were set to 48°C and − 1°C for woody savanna, and 48°C and 0°C for grassland, respectively (Zhang et al., 2017).

In comparison to VPM v1.0 and VPM v.2.0 which used the $TA_{opt\text{-}biome}$ parameter, VPM v3.0 used the $TA_{opt\text{-}site}$ parameter. The methods to estimate $TA_{opt\text{-}site}$ with GPP_{EC} and MODIS images at individual EC tower sites were reported in previous publications (Chang et al., 2020; Chang et al., 2021; Pan et al., 2024). The $TA_{opt\text{-}site}$ value is calculated based on the response curves of GPP_{EC} versus $TA_{DT\text{-}ERA5}$ and EVI versus $TA_{DT\text{-}ERA5}$. Both GPP_{EC} and EVI increased with an increase in $TA_{DT\text{-}ERA5}$, reached a peak, and then declined as an increase in $TA_{DT\text{-}ERA5}$ (Fig. 2). For the $TA_{opt\text{-}site}$ value calculation, first, we found the maximum GPP_{EC} and EVI values for each site, respectively. Then, $TA_{opt\text{-}site}$ was calculated as the mean $TA_{DT\text{-}ERA5}$ value during those GPP_{EC} or EVI observations equal to or higher than 95% maximum GPP_{EC} and EVI (Chang et al., 2020; Chang et al., 2021). Table 2 lists the differences between the $TA_{opt\text{-}site}$ calculated by GPP_{EC} and EVI. The $TA_{opt\text{-}site}$ values varied among the five sites and showed some differences with $TA_{opt\text{-}biome}$. Considering EVI data are available globally and GPP_{EC} data are only available in EC tower sites, we selected $TA_{opt\text{-}site\text{-}EVI}$ as the input for the VPM model simulations, which could help us to carry out global simulations of the VPM model in the future.

The W_{scalar} was calculated as

$$W_{scalar} = \frac{1+LSWI}{1+LSWI_{max}}, \quad (7)$$

where $LSWI_{max}$ is the largest LSWI value during the growing season (April to October at US-WKG, US-SRG, and US-SRM sites, and the whole year at US-VAR and US-TON sites) within one year. Equation (7) was reported to have good performance in semi-humid and humid areas (Xiao et al., 2004a; Yan et al., 2009) but would underestimate the degree (severity) of water stress on photosynthesis under the very dry conditions in arid and semi-arid areas (He et al., 2014). As shown in Fig. 3, long-term mean LSWI values were lower than −0.1

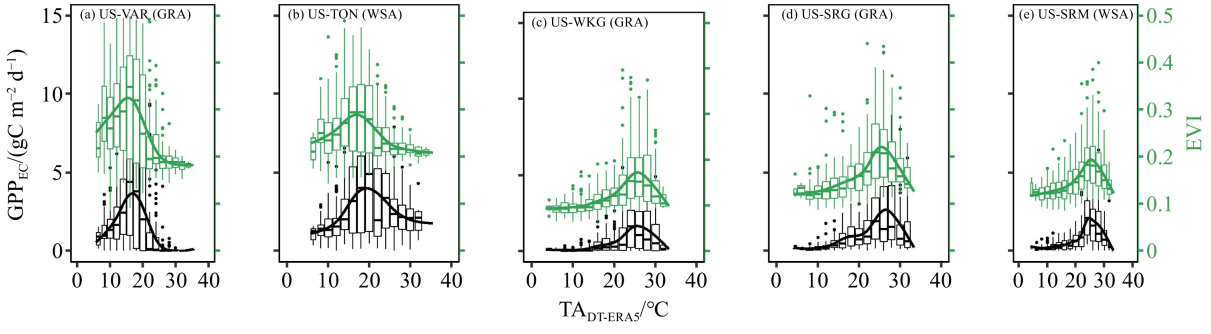

Fig. 2 The relationships between daily daytime mean air temperature ($TA_{DT\text{-}ERA5}$), eddy covariance-derived daily gross primary production (GPP_{EC}), and enhanced vegetation index (EVI) at the five flux tower sites. The solid black and green lines are fitting curves for GPP_{EC} and EVI using a cyclic penalized cubic regression spline. The data was binned for 2°C intervals.

Table 2 Summary of site-specific optimum air temperature (TA_{opt}) for photosynthesis at the five study sites

Study sites	US-VAR	US-TON	US-WKG	US-SRG	US-SRM
$TA_{opt\text{-}biome}$ (°C)	27	24	27	27	24
$TA_{opt\text{-}site\text{-}GPP}$ (°C)	18	19	25	28	28
$TA_{opt\text{-}site\text{-}EVI}$ (°C)	16	16	26	26	26
$TA_{opt\text{-}site\text{-}GPP} - TA_{opt\text{-}site\text{-}EVI}$ (°C)	2	3	−1	2	2
$TA_{opt\text{-}site\text{-}EVI} - TA_{opt\text{-}biome}$ (°C)	−11	−8	−1	−1	2
$TA_{opt\text{-}site\text{-}GPP} - TA_{opt\text{-}biome}$ (°C)	−9	−5	−2	1	4

Notes: $TA_{opt\text{-}biome}$: optimum air temperature based on biome-specific lookup-table; $TA_{opt\text{-}site\text{-}GPP}$: optimum air temperature estimated from GPP_{EC}, $TA_{opt\text{-}site\text{-}EVI}$: optimum air temperature estimated from EVI.

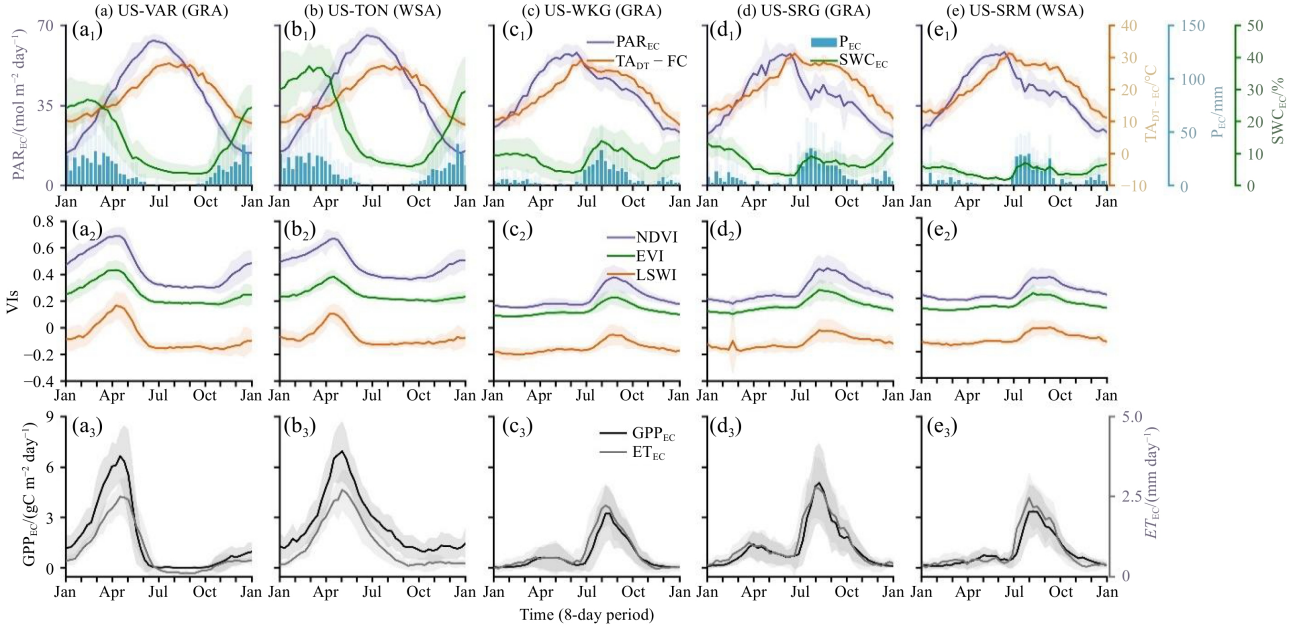

Fig. 3 Seasonal dynamics of photosynthetically active radiation from EC observations (PAR_{EC}), mean daytime air temperature from EC observations ($TA_{DT\text{-}EC}$), precipitation from EC observations (P_{EC}), soil water content (SWC_{EC}) from EC observations, three vegetation indices (VIs), eddy covariance-derived gross primary production (GPP_{EC}), eddy covariance-measured evapotranspiration (ET_{EC}) at five flux tower sites. The curves shown in this figure are mean values for multi-year based on the site data availability, and the shadow represents the +/−1 standard deviation.

during the very dry period at these sites. Thus, we applied the modified W_{scalar} equation under very dry conditions, using the same procedure reported in our previous publications (He et al., 2014; Wagle et al., 2015b):

$$W_{scalar} = 0.5 + LSWI. \quad (8)$$

When LSWI value was lower than −0.1, which represents a dry condition, we applied Eq. (8) in the VPM simulation. This modification improves the accuracy of water stress estimation by better reflecting the severity of water limitation on photosynthesis. For example, on June 17, 2008, the US-WKG site had an LSWI value of −0.155, and W_{scalar} calculated by Eq. (7) was 0.83 but W_{scalar} calculated by Eq. (8) was 0.35, which more accurately accounted for the degree of water stress on GPP.

2.3.2 The Vegetation Transpiration Model (VTM v2.0)

The VTM was developed to estimate daily transpiration (mm H_2O /day), based on the intrinsic coupling between photosynthesis and transpiration processes at the leaf scale, i.e., water use efficiency (WUE) (Eq. (9)), and it combines the inverse of WUE and GPP to estimate transpiration (T) (Alfieri et al. 2009; Pan et al. 2024). The equation can be described as follows:

$$WUE = GPP/Transpiration, \quad (9)$$

$$T = \frac{1}{WUE} \times GPP_{VPM}, \quad (10)$$

$$\frac{1}{WUE} = C3F \times \frac{1}{WUE_{C3}} + C4F \times \frac{1}{WUE_{C4}}. \quad (11)$$

At the leaf level, 1/WUE = 0.27 mm H_2O/g C for the

C3 plant and 0.135 mm H_2O/g C for the C4 plant, respectively (Nobel, 2020). More details about the 1/WUE can be found in supplementary materials for Method 1. The GPP data from the simulations of VPM (GPP_{VPM}) in an 8-day temporal interval was used to estimate T ($mm \cdot day^{-1}$).

2.3.3 Simulation of VPM and VTM models

In this study, two meteorological data sets: *in situ* meteorological data from the EC tower and reanalysis meteorological data from the ERA5 data set were used to drive VPM and VTM simulations. These two meteorological data sets were averaged over an 8-day interval, matching the temporal resolution of MODIS composite images using the equations in Sections 2.3.1 and 2.3.2, and were used to run VPM and VTM. For the *in situ* meteorological data set, the model simulation was dependent on the data availability. For the ERA5 reanalysis data set, we simulated VPM and VTM from 2000 to 2021 (22 years). We defined active growing season as GPP > 1 g $C \cdot m^{-2} \cdot day^{-1}$ for model evaluation (Wagle et al., 2014).

2.4 Statistical data analysis

Three statistical metrics: regression coefficient (α), the coefficient of determination (R^2), and root mean square error (*RMSE*) were calculated to assess the accuracies and uncertainties of the model simulations. The R^2 value denotes the amount of variation in the measurements that could be predicted by the estimates, and the *RMSE* expresses the differences between the estimates and the measurements.

Mean annual environmental factors data, vegetation indices, GPP, and T were calculated as the averaged value of each variable over their temporal coverage. The interannual trends of vegetation indices, GPP, T, and climate in this study were analyzed by using the Mann-Kendall test and Sen's method. The Mann-Kendall test was used to evaluate the reliability of the results (Mann, 1945; Kendall, 1948), while Sen's slope method was used to quantify the trends (Sen, 1968).

3 Results

3.1 Seasonal dynamics of environmental factors, vegetation indices, and carbon and water fluxes

Figure 3 shows the averaged seasonal dynamics of PAR_{EC}, $TA_{DT\text{-}EC}$, P_{EC}, SWC_{EC}, vegetation indices, GPP_{EC}, and ET_{EC} at the five sites. With the Mediterranean climate in California, USA, the grassland site (US-VAR) and woody savanna site (US-TON) had similar seasonal dynamics of PAR_{EC} and $TA_{DT\text{-}EC}$. They started to increase in spring and reached their peaks in summer. The seasonal dynamics of precipitation were characterized by a dry season from late spring to early fall and a wet season from late fall to spring. SWC_{EC} at the woody savanna site was higher than the grassland site, with low SWC_{EC} in the summer (< 10%) and high SWC_{EC} in winter and spring (up to 45%). Vegetation indices (VIs, NDVI, EVI, and LSWI) had similar seasonal dynamics, characterized by a peak in spring. Both GPP_{EC} and ET_{EC} had similar seasonal dynamics, characterized by a peak in spring. The seasonal dynamics of GPP_{EC} and ET_{EC} agreed well with the seasonal dynamics of VIs. The period of $GPP_{EC} \geqslant 1$ g $C \cdot m^{-2} \cdot day^{-1}$ (early March – July at the woody savanna site, February–May at the grassland site) corresponded well with the period with increased vegetation indices (i.e., an indication of growing seasons).

Under the monsoon climate in southern Arizona, USA, the grassland sites (US-WKG (Fig. 3(c)), US-SRG (Fig. 3(d)) and woody savanna site (US-SRM, Fig. 3(e)) had similar seasonal dynamics of environmental factors. PAR_{EC} and $TA_{DT\text{-}EC}$ reached their peak values in June and decreased gradually in summer. The seasonal dynamics of precipitation were characterized by dry spring and fall seasons, a moderately wet winter (November–February), and a wetter monsoon (July–October). SWC_{EC} was relatively high from July to February and low from March to June. Three VIs (NDVI, EVI, and LSWI) had similar seasonal dynamics, characterized by a large peak period in August–September. GPP_{EC} and ET_{EC} had similar seasonal dynamics, with moderate values in the spring growing season and larger values in the summer growing season.

3.2 Comparisons of GPP_{EC} and GPP_{VPM} from the VPM simulation

A comparison between GPP_{EC} and GPP_{VPM} is shown in Fig. 4. In general, both $GPP_{VPM\text{-}EC}$ and $GPP_{VPM\text{-}ERA5}$ tracked the seasonal dynamics of GPP_{EC} reasonably well at the five sites. Specifically, for the two sites under the Mediterranean climate (Figs. 4(a1) and 4(b1)), both $GPP_{VPM\text{-}EC}$ and $GPP_{VPM\text{-}ERA5}$ precisely tracked the dynamics of GPP_{EC} from February to June but showed moderate differences from July to October. For the three monsoon sites (Figs. 4(c1) and 4(e1)), both $GPP_{VPM\text{-}EC}$ and $GPP_{VPM\text{-}ERA5}$ agreed reasonably well with GPP_{EC} during the summer growing season (July to October), $GPP_{VPM\text{-}EC}$ showed slight differences in May–June with GPP_{EC}, while the $GPP_{VPM\text{-}ERA5}$ showed noticeable difference. Linear regression showed a high correlation of $GPP_{VPM\text{-}EC}$ and $GPP_{VPM\text{-}ERA5}$ with GPP_{EC}, with R^2 values ranging from 0.76 to 0.93 and *RMSE* values ranging from 0.8 to 1.7 g $C \cdot m^{-2} \cdot day^{-1}$. The linear regression slope values between $GPP_{VPM\text{-}EC}$ and GPP_{EC} differ among the sites: −10% for US-TON, +2% for US-VAR, +5% for

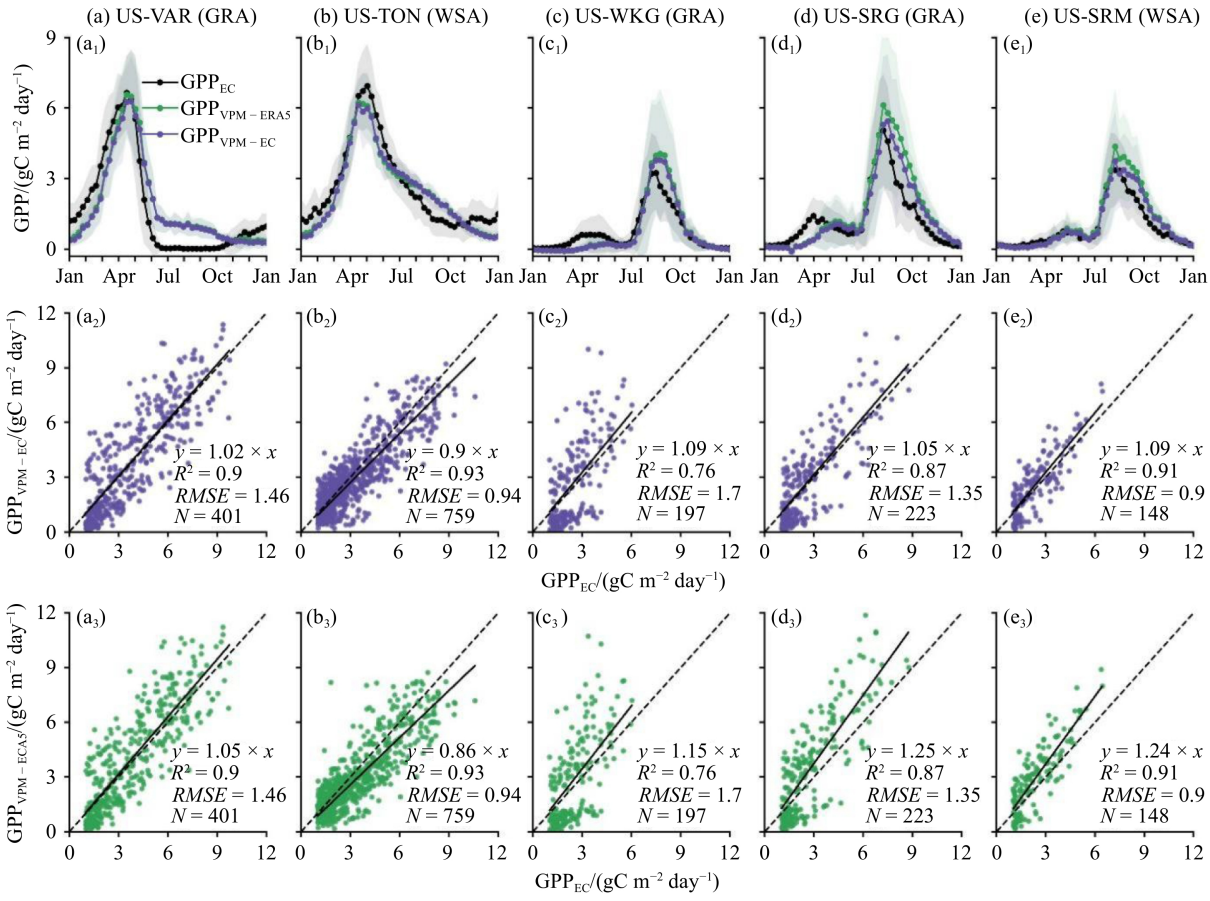

Fig. 4 Seasonal dynamics (top panel) and linear comparisons (middle and bottom panels) between eddy covariance-derived gross primary production (GPP_{EC}) and vegetation photosynthesis model-based GPP estimates using *in situ* climate data (GPP_{VPM-EC}) and ERA5 reanalysis climate data ($GPP_{VPM-ERA5}$) at the five flux tower sites. The shadow in the first panel plots is the standard deviation of the means when averaged for the study period.

US-SRG, and +9% for both US-WKG and US-SRM. The VPM driven by ERA5 data showed slightly larger differences: −14% for US-TON, +5% for US-VAR, +15% for US-WKG, and +25% for both US-SRG and US-SRM.

3.3 Temporal consistency of evapotranspiration and transpiration at temporal scales of 8-day period

The seasonal dynamics of T_{VTM-EC} and $T_{VTM-ERA5}$ matched reasonably well with the seasonal dynamics of ET_{EC} (Fig. 5). However, there were large differences in their magnitudes. Linear regression showed a strong correlation of T_{VTM-EC} and $T_{VTM-ERA5}$ with ET_{EC}, with R^2 values ranging from 0.69 to 0.92, and *RMSE* ranging from 0.21 to 0.37 mm·day^{-1}. The T_{VTM-EC} / ET_{EC} ratio varies across the sites, ranging from 0.71 for US-VAR and 0.61 for US-TON under Mediterranean climate, to 0.29 for US-SRM, 0.27 for US-SRG and 0.23 for US-WKG, which is in the monsoon climate area. The $T_{VTM-ERA5}$ / ET_{EC} ratios showed similar differences with T_{VTM-EC} / ET_{EC}, ranging from 0.27 to 0.73 at the five sites.

3.4 Comparison between annual GPP_{EC} vs. GPP_{VPM} and annual ET_{EC} vs. T_{VTM}

A comparison between the annual GPP_{EC} and GPP_{VPM} is shown in Fig. 6. The difference between the regression slopes for annual GPP_{EC} versus GPP_{VPM-EC} was within 11% of the 1-1 line at the five sites. Results were similar to $GPP_{VPM-ERA5}$. At the US-SRG and US-SRM sites, the differences between annual GPP_{EC} and $GPP_{VPM-ERA5}$ (26% and 25% difference at the US-SRG and US-SRM sites, respectively) were noticeably higher than those between GPP_{EC} and GPP_{VPM-EC} (6% and 11% difference at the US-SRG and US-SRM site, respectively).

At the annual scale, the ratio of annual T_{VTM-EC} and annual ET_{EC} varied among the five sites (0.68 at the US-VAR, 0.65 at the US-TON, 0.30 at the US-SRM, 0.26 at the US-SRG, and 0.22 at the US-WKG). Results were similar for ET_{EC} and $T_{VTM-ERA5}$. The ratio of annual $T_{VTM-ERA5}$ and annual ET_{EC} was 0.70 at the US-VAR site, 0.63 at the US-TON site, 0.34 at the US-SRM site, 0.31 at the US-SRG site, and 0.23 at the US-WKG site.

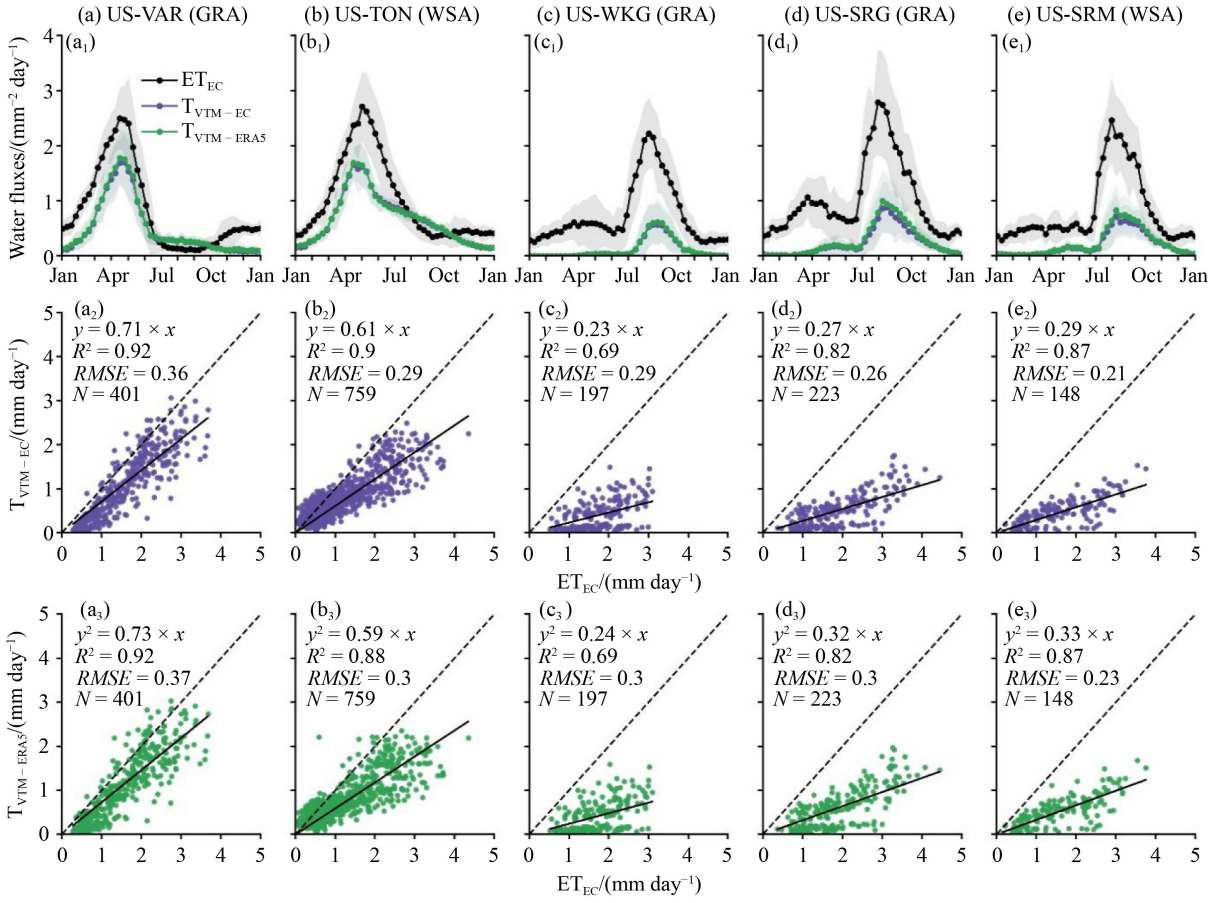

Fig. 5 Seasonal dynamics (top panel) and linear correlation (middle and bottom panel) between eddy covariance-measured evapotranspiration (ET_{EC}) and vegetation transpiration model-based transpiration (T) estimate using *in situ* climate data ($T_{VTM\text{-}EC}$) and ERA5 reanalysis climate data ($T_{VTM\text{-}ERA5}$) at the five flux tower sites. The shadow in the first panel plots is the standard deviation of the means when averaged for the study period.

3.5 Interannual variability of atmospheric CO_2, environmental factors, VIs, gross primary production, and transpiration during 2000–2021

The interannual variability of atmospheric CO_2 concentration, environmental factors (PAR_{ERA5}, $TA_{DT\text{-}ERA5}$, and P_{ERA5}), vegetation indices (NDVI, EVI, and LSWI), GPP_{VPM}, and T_{VTM} during 2000−2021 at the five sites are shown in Fig. 7. Atmospheric CO_2 concentration showed a significant increasing trend. The Sen's slope ranged from 2.16 ppm·yr^{-1} to 2.48 ppm·yr^{-1} among the five sites. Daytime air temperature showed a significant increasing trend (Sen's slope: 0.05). PAR_{ERA5} and P_{ERA5} showed no significant trend. EVI at the US-SRM site showed significant increasing trends.

The $GPP_{VPM\text{-}ERA5}$ and $T_{VTM\text{-}ERA5}$ exhibited no significant trend during 2000−2021 at one savanna and three grassland sites, but they increased substantially at the US-SRM savanna site. At the US-SRM, $GPP_{VPM\text{-}ERA5}$, and $T_{VTM\text{-}ERA5}$ showed an increasing trend of 10.59 g C·m^{-2}·yr^{-1} and 2.0 mm H_2O·yr^{-1}, respectively. The Mediterranean climate sites had the highest GPP and T followed by the US-SRG grassland site and the US-SRM savanna site. The US-WKG grassland had the smallest GPP and T.

4 Discussion

4.1 Improvement of the VPM and GPP_{VPM} estimation

The VPM v2.0 was applied to generate a global GPP data set over the years 2000−2016, which was released to the public and used by the research community (Zhang et al., 2017). Both VPM v2.0 and the MOD17 GPP data products (Running and Zhao, 2019) use biome-specific $TA_{opt\text{-}biome}$ parameters for photosynthesis. Previous studies revealed the limitation of biome-specific $TA_{opt\text{-}biome}$ in the LUE-based GPP models and showed the need and potential of using site-specific $TA_{opt\text{-}site}$ to improve GPP estimates in VPM (Chang et al., 2020, 2021). In this study, we used the same method from the previous publications (Chang et al., 2020, 2021) to estimate site-specific $TA_{opt\text{-}site}$. In comparison to the previous publications that used a few years of data, this study used longer time series data (11 to 21 years) and

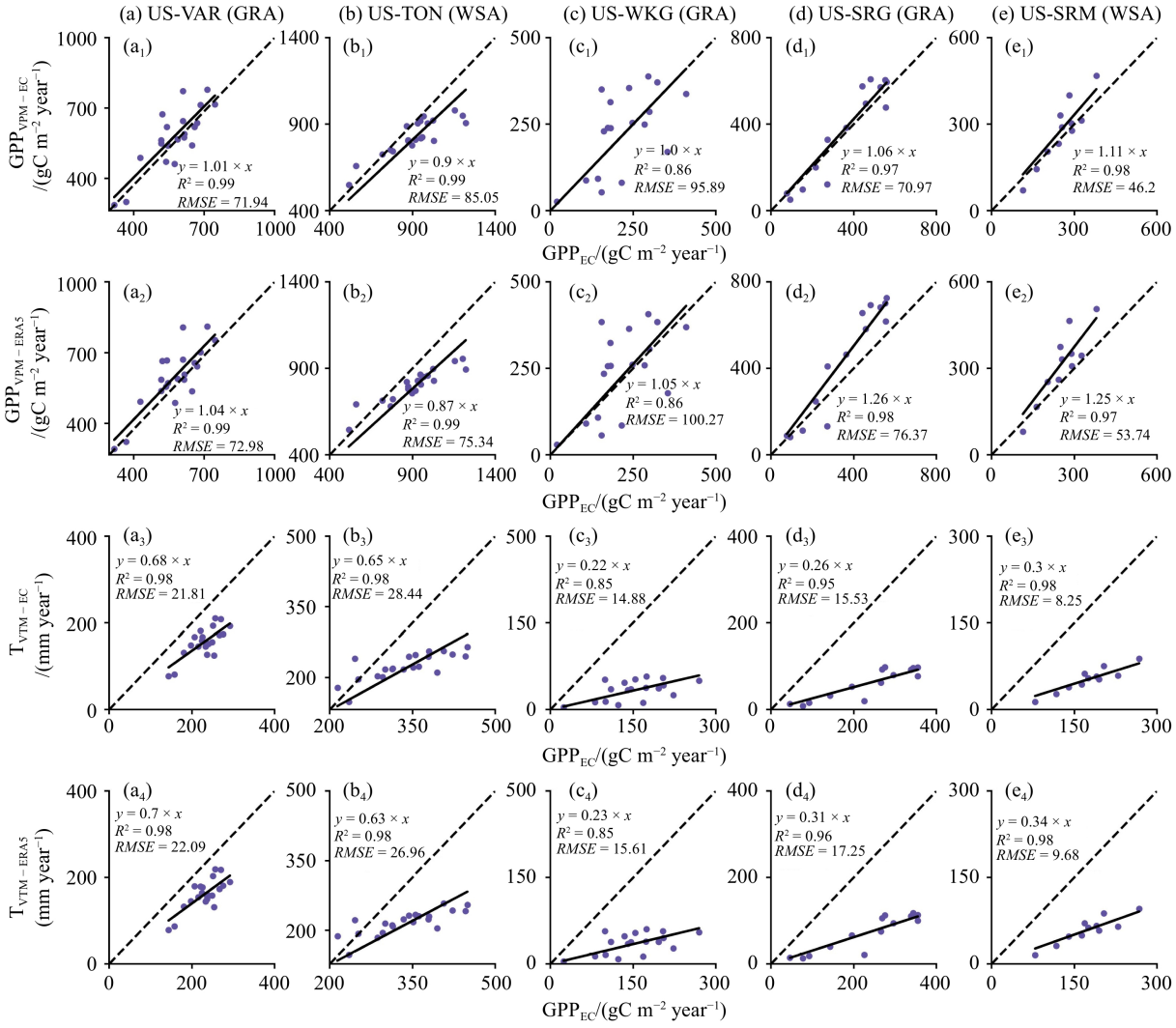

Fig. 6 Relationship between active growing season sums of eddy covariance-derived gross primary production (GPP_{EC}) and vegetation photosynthesis model-based GPP, eddy covariance-measured evapotranspiration (ET_{EC}), and vegetation transpiration model-based transpiration (T).

confirmed that $TA_{opt\text{-}site}$ values calculated from the relationship between GPP_{EC} and $TA_{DT\text{-}ERA5}$ were consistent with $TA_{opt\text{-}site}$ values from the relationship between EVI and $TA_{DT\text{-}ERA5}$. The VPM simulation results demonstrated the potential of using $TA_{opt\text{-}site}$ to replace $TA_{opt\text{-}biome}$ for improving GPP estimation by the VPM. The use of EVI in estimating $TA_{opt\text{-}site}$ has great potential for improving global VPM modeling as time series satellite-derived EVI data are available globally.

The discrepancies between GPP_{VPM} and GPP_{EC} in some periods can be attributed to several sources of errors and uncertainties. First, climate data (e.g., PAR) affect model simulations (He et al., 2014). PAR is one of the most sensitive input variables of the VPM model (He et al., 2014). In this study, PAR_{ERA5} exhibited larger differences with PAR_{EC} at the US-SRG (11% difference) and US-SRM (14% difference) sites than the other three sites. These differences propagate to GPP_{VPM} driven by ERA5 climate data, resulting in much larger discrepancies with GPP_{EC} than did GPP_{VPM} driven by EC climate data at these two sites. It highlights the need for careful quality control of PAR data and suggests that an empirical or semi-empirical correction may be needed when using the ERA5 as model input data. Second, the time series of vegetation index data often have missing (bad quality) data due to clouds, aerosol, and other noise, and how to gap-fill the missing data for a complete time series of remote sensing data is still under debate (Shen et al., 2015). The time lag of EVI when drought occurs also introduces biases to VPM simulation (Dong et al., 2015). For example, at the US-SRG site, there was moderate disagreement between GPP_{EC} and GPP_{VPM} during the spring dry period (April – June). In this site, there is a prominent dry period from April to June. When drought occurs, even at similar light conditions from morning to afternoon hours, photosynthesis could decrease considerably due to stomatal closure (Wagle and Kakani, 2014). However, significant alterations in pigment

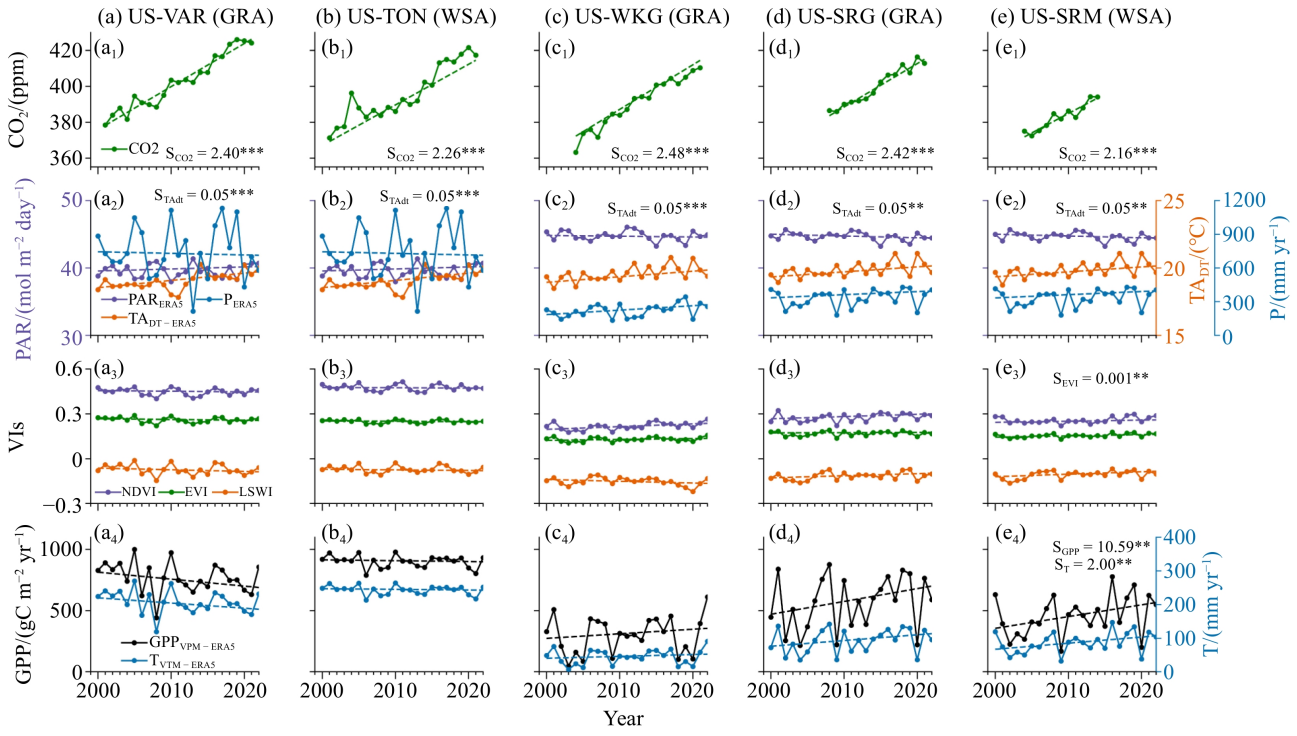

Fig. 7 Interannual variation and trend of atmospheric CO_2 concentration, climate (PAR_{ERA5}, $TA_{DT\text{-}ERA5}$, and P_{ERA5}), vegetation indices (NDVI, EVI, and LSWI), $GPP_{VPM\text{-}ERA5}$, and $T_{VTM\text{-}ERA5}$. S means the Sen's slope. ** indicates significant at $P = 0.05$ level, *** indicates significant at $P = 0.001$ level. PAR_{ERA5}: photosynthetically active radiation. $TA_{DT\text{-}ERA5}$: daytime air temperature, P_{ERA5}: precipitation, NDVI: Normalized Difference Vegetation Index, EVI: Enhanced Vegetation Index, LSWI: Land Surface Water Index, $GPP_{VPM\text{-}ERA5}$: gross primary production estimates from ERA5 data-driven VPM, $T_{VTM\text{-}ERA5}$: transpiration estimates from ERA5 data-driven VTM.

concentration and canopy structure, such as leaf shedding and reductions in leaf area index, which influence NDVI and EVI, typically require several days to several weeks to become noticeable. Due to the time lag of EVI, the simulated GPP peaked slightly later than the peak GPP_{EC} during the spring dry period.

Third, various proportions of trees and grasses occurred in three of the five sites in this study, and various proportions of C3 and C4 grasses also occurred at the study sites. C3 and C4 plants have different photosynthetic pathways, which leads to different LUE values. In the VPM, the proportions of C3 and C4 plants in a grassland or savanna affect the maximum LUE parameter ($LUE_0 = C3F \times LUE_{0\text{-}C3} + C4F \times LUE_{0\text{-}C4}$). However, it is difficult to measure or estimate accurately species composition, which changes over time. Two approaches have been used to estimate C3/C4 ratios in grasslands and savannas: 1) make an educated guess of C3/C4 mixing ratios based on site-specific knowledge or 2) use known C3/C4 ratios from other data sources (*in situ* observations or model-based estimation). As the US-WKG, US-SRG, and US-SRM sites do not have sufficient information on varying mixing ratios of C3 and C4 grasses, we estimated C3/C4 plant ratios based on available plant cover estimates, which may contribute to the moderate discrepancies between GPP_{EC} and GPP_{VPM}. Additionally, fixed proportions of C3 and C4 species do not account for seasonal changes in species composition. For example, C4 plants might dominate in hotter, drier conditions typically found in summer, while C3 plants might be more prevalent in cooler, wetter conditions. Fixed C3/C4 ratios fail to reflect these shifts, potentially leading to over- or underestimation of GPP_{VPM} during specific periods. To date, the capacity to model and predict spatial distribution and temporal (seasonal and inter-annual) abundance of C4 plants across the scales from local to global is still poor (Still et al., 2003; Winslow et al., 2003; Luo et al., 2024). The result of this study further highlights the need to model and generate accurate local regional and global C4 plant distribution maps in the future. The fourth uncertainty could be attributed to the estimation error of GPP_{EC}. For example, during the summer, EVI at the US-VAR site was close to 0.2, which indicated the presence of green vegetation. Many studies have shown EVI > 0.1 can be an indicator of green vegetation (Xiao et al., 2009; Wang et al., 2020). However, GPP_{EC} at the US-VAR site during this period was almost zero. This causes a moderate disagreement between GPP_{EC} and GPP_{VPM} at this site during summer.

4.2 The range of T/ET ratios in grasslands and savanna

Due to the lack of *in situ* T measurement for model validation, we compared the T or T/ET ratio estimates

across the five sites with published studies using several methods. A previous study reported T of 281 mm·yr^{-1} and T/ET of 0.6 at the US-TON site, based on EC tower measurements of above and below the tree canopy for ET partition (Ma et al., 2020). Based on modeling results, Ma et al. (2020) reported that at the US-TON site, T/ET ratio varies from 0.74 (with the assumption of t = 0 if GPP = 0) to 0.39 (with the assumption of the linear relationship between GPP and ET). Our results were within these ranges, with multi-year averages of T of 243 mm·yr^{-1} and T/ET of 0.69, respectively. Similarly, at the US-VAR grassland site, the T/ET ratio ranged from 0.66 (with the assumption of t = 0 if GPP = 0) to 0.47 (with the assumption of the linear relationship between GPP and ET) (Ma et al., 2020). Our analysis yielded a T/ET$_{EC}$ ratio of 0.70 at the US-VAR Mediterranean grassland site. By using the x-axis intercepts for ET vs GPP as an estimate of evaporation (E), and by subtracting E from ET measured by the EC tower, the annual mean T/ET ratio was 0.62 at the US-SRM woody savanna site, 0.58 at the US-SRG grassland site, and 0.55 at the US-WKG grassland site, respectively (Scott et al., 2015). Scott and Biederman (2017) applied this method to monthly growing-season ET partitioning and predicted that T/ET ratio ranged from 0.45 to 0.69 (mean of 0.62, July–October) at the US-SRM site, from 0.51 to 0.62 (mean of 0.55, July–October) at the US-SRG site, and from 0.26 to 0.58 (mean of 0.46, July–October) at the US-WKG site, respectively. Our T/ET$_{EC}$ ratio estimates at the US-SRM, US-SRG, and US-WKG sites (0.23 to 0.29) were substantially lower than these results.

In this study, we conducted preliminary work on using VTM to estimate T. This simple method, which assumes a constant WUE, performed reasonably at the US-VAR and US-TON sites but was less effective at the US-WKG, US-SRG, and US-SRM sites. The WUE may be affected by different factors such as climate, soil moisture, plant functional types, etc. (Cooley et al. 2022). These factors might restrict the model's effectiveness and precision when applied to various ecosystems and climatic areas. The limitation suggests that it is a challenging task to accurately estimate T using such a simple approach. It is clear that the magnitude of T estimates needs to be further evaluated, and water use efficiency or transpiration ratio parameters need to be carefully evaluated, too, especially in sparse vegetation ecosystems under semiarid and arid environments.

4.3 Interannual variability of GPP and T

In grassland and savanna ecosystems, GPP is impacted by environmental factors such as atmospheric CO_2 concentration, air temperature, precipitation, and solar radiation. Increasing atmospheric CO_2 concentration could increase GPP but reduce the T of grassland and savanna (CO_2 fertilization effect). A previous study found that no interannual trend in ET or oak canopy T was observed using the EC method at the US-TON woody savanna and the US-VAR grassland site from 2001 through 2019 despite an increasing trend of atmospheric CO_2 concentration and an increasing trend of air temperature and large variability of annual precipitation (ranging from 133 to 890 mm·yr^{-1}) (Baldocchi et al., 2021). We also found no interannual trend of GPP derived from the EC tower from 2001 to 2021 at these two sites (Fig. S3). The US-SRG grassland sites also showed no interannual trend of GPP during 14 years of *in situ* observations. Consistent with the observation results, our model simulation showed no significant trends of GPP and T over the last 22 years (2000−2021) at the US-TON woody savanna, US-VAR grassland, and US-SRG grassland sites. At the US-WKG grassland site, GPP$_{EC}$ showed a significant increasing trend from 2004 to 2021, but VPM simulation results showed no significant trend from 2000 to 2021. Our VPM simulation results showed a significant increase in GPP from 2000 to 2021 at the US-SRM savanna site, which aligns with the trend of GPP$_{EC}$ rising from 2004 to 2022 (Scott et al., 2023). This trend can be attributed to the increasing overstory woody plant cover and understory grass cover (Scott et al., 2023). The observed trends and interannual variability in GPP and T highlight the importance of continuous observation and modeling, which can guide effective land management strategies, ensuring the sustainability of these vital ecosystems.

5 Conclusions

In this study, we employed VPM and VTM to estimate GPP and T, respectively. We explored the seasonal dynamics, interannual variability, and decadal trends of atmospheric CO_2 concentration, environmental factors, vegetation indices, GPP, and T across five savanna and grassland sites. VPM demonstrated good performance in capturing the seasonal dynamics and interannual variability of GPP$_{EC}$. Using EVI as an alternative to EC-derived GPP to estimate the TA$_{opt}$ for photosynthesis has improved the VPM simulation. Employing ERA5 reanalysis data as inputs for VPM simulations aligned well with site EC-observed results, supporting the potential of VPM simulations at regional and global scales. The VTM effectively tracked the seasonal dynamics of ET in savanna and grassland, though additional parameterization is needed for this simple leaf-level WUE approach to accurately estimate T in different climate zones. This study combines climate and satellite data to simulate long-term carbon and water fluxes, the results align well with eddy covariance observation, which plays a vital role in understanding the carbon and water cycles in response to atmospheric CO_2 concentration increase and climate change. By scaling up

this methodology, the VPM model could become a valuable tool for estimating GPP in grasslands and savannas on regional to global scales, thereby supporting grassland management and conservation efforts under climate change scenarios.

Electronic Supplementary Material is available in the online version of this article at https://doi.org/10.1007/s11707-024-1136-8 and is accessible for authorized users.

Acknowledgments This study was supported by research grant from the US National Science Foundation (OIA-1946093). We thank Dr. Dennis Baldocchi at the University of California, Berkeley for his suggestions and eddy flux tower sites data in the manuscript. We thank three anonymous reviewers for their time and effort in the review of our earlier version of this manuscript. Data collection at these AmeriFlux sites is supported in part by the US Department of Energy's Office of Science. Data for these AmeriFlux sites can be downloaded from FLUXNET2015 website.

Competing interests The authors declare that they have no competing interests.

References

Alfieri J G, Xiao X, Niyogi D, Pielke R A Sr, Chen F, LeMone M A (2009). Satellite-based modeling of transpiration from the grasslands in the Southern Great Plains, USA. Global Planet Change, 67(1−2): 78–86

Baldocchi D (2014). Measuring fluxes of trace gases and energy between ecosystems and the atmosphere – The state and future of the eddy covariance method. Glob Change Biol, 20(12): 3600–3609

Baldocchi D, Ma S, Verfaillie J (2021). On the inter- and intra-annual variability of ecosystem evapotranspiration and water use efficiency of an oak savanna and annual grassland subjected to booms and busts in rainfall. Glob Change Biol, 27(2): 359–375

Biederman J A, Scott R L, Bell T W, Bowling D R, Dore S, Garatuza-Payan J, Kolb T E, Krishnan P, Krofcheck D J, Litvak M E, Maurer G E, Meyers T P, Oechel W C, Papuga S A, Ponce-Campos G E, Rodriguez J C, Smith W K, Vargas R, Watts C J, Yepez E A, Goulden M L (2017). CO_2 exchange and evapotranspiration across dryland ecosystems of southwestern North America. Glob Change Biol, 23(10): 4204–4221

Chang Q, Xiao X, Doughty R, Wu X, Jiao W, Qin Y (2021). Assessing variability of optimum air temperature for photosynthesis across site-years, sites and biomes and their effects on photosynthesis estimation. Agric For Meteorol, 298–299: 108277

Chang Q, Xiao X, Wu X, Doughty R, Jiao W, Bajgain R, Qin Y, Wang J (2020). Estimating site-specific optimum air temperature and assessing its effect on the photosynthesis of grasslands in mid- to high-latitudes. Environ Res Lett, 15(3): 034064

Cooley S S, Fisher J B, Goldsmith G R (2022). Convergence in water use efficiency within plant functional types across contrasting climates. Nat Plants, 8(4): 341–345

Dong J, Xiao X, Wagle P, Zhang G, Zhou Y, Jin C, Torn M S, Meyers T P, Suyker A E, Wang J, Yan H, Biradar C, Moore B III (2015). Comparison of four EVI-based models for estimating gross primary production of maize and soybean croplands and tallgrass prairie under severe drought. Remote Sens Environ, 162: 154–168

Dye D G (2004). Spectral composition and quanta-to-energy ratio of diffuse photosynthetically active radiation under diverse cloud conditions. J Geophys Res, 109(D10): 2003JD004251

Gentine P, Green J K, Guérin M, Humphrey V, Seneviratne S I, Zhang Y, Zhou S (2019). Coupling between the terrestrial carbon and water cycles—a review. Environ Res Lett, 14(8): 083003

Goetz S J, Prince S D, Goward S N, Thawley M M, Small J (1999). Satellite remote sensing of primary production: an improved production efficiency modeling approach. Ecol Modell, 122(3): 239–255

He H, Liu M, Xiao X, Ren X, Zhang L, Sun X, Yang Y, Li Y, Zhao L, Shi P, Du M, Ma Y, Ma M, Zhang Y, Yu G (2014). Large-scale estimation and uncertainty analysis of gross primary production in Tibetan alpine grasslands. J Geophys Res Biogeosci, 119(3): 466–486

Huete A R, Liu H Q, Batchily K, van Leeuwen W (1997). A comparison of vegetation indices over a global set of TM images for EOS-MODIS. Remote Sens Environ, 59(3): 440–451

Huete A, Didan K, Miura T, Rodriguez E P, Gao X, Ferreira L G (2002). Overview of the radiometric and biophysical performance of the MODIS vegetation indices. Remote Sens Environ, 83(1−2): 195–213

Jiang C, Ryu Y (2016). Multi-scale evaluation of global gross primary productivity and evapotranspiration products derived from Breathing Earth System Simulator (BESS). Remote Sens Environ, 186: 528–547

Kemp D R, Guodong H, Xiangyang H, Michalk D L, Fujiang H, Jianping W, Yingjun Z (2013). Innovative grassland management systems for environmental and livelihood benefits. Proc Natl Acad Sci USA, 110(21): 8369–8374

Kendall M G (1948). Rank Correlation Methods. Griffin, Oxford: England

Konapala G, Mishra A K, Wada Y, Mann M E (2020). Climate change will affect global water availability through compounding changes in seasonal precipitation and evaporation. Nat Commun, 11(1): 3044

Li X, Gentine P, Lin C, Zhou S, Sun Z, Zheng Y, Liu J, Zheng C (2019). A simple and objective method to partition evapotranspiration into transpiration and evaporation at eddy-covariance sites. Agric For Meteorol, 265: 171–182

Luo X, Zhou H, Satriawan T W, Tian J, Zhao R, Keenan T F, Griffith D M, Sitch S, Smith N G, Still C J (2024). Mapping the global distribution of C4 vegetation using observations and optimality theory. Nat Commun, 15(1): 1219

Ma S, Baldocchi D, Wolf S, Verfaillie J (2016). Slow ecosystem responses conditionally regulate annual carbon balance over 15 years in Californian oak-grass savanna. Agric For Meteorol, 228–229: 252–264

Ma S, Eichelmann E, Wolf S, Rey-Sanchez C, Baldocchi D D (2020). Transpiration and evaporation in a Californian oak-grass savanna: field measurements and partitioning model results. Agric For Meteorol, 295: 108204

Mann H B (1945). Nonparametric tests against trend. Econometrica, 13(3): 245–259

Nelson J A, Pérez-Priego O, Zhou S, Poyatos R, Zhang Y, Blanken P D, Gimeno T E, Wohlfahrt G, Desai A R, Gioli B, Limousin J M, Bonal D, Paul-Limoges E, Scott R L, Varlagin A, Fuchs K, Montagnani L, Wolf S, Delpierre N, Berveiller D, Gharun M, Belelli Marchesini L, Gianelle D, Šigut L, Mammarella I, Siebicke L, Andrew Black T, Knohl A, Hörtnagl L, Magliulo V, Besnard S, Weber U, Carvalhais N, Migliavacca M, Reichstein M, Jung M (2020). Ecosystem transpiration and evaporation: insights from three water flux partitioning methods across FLUXNET sites. Glob Change Biol, 26(12): 6916–6930

Nobel P S (2020) Physicochemical and Environmental Plant Physiology (5th Ed). New York: Academic Press

O'Mara F P (2012). The role of grasslands in food security and climate change. Ann Bot (Lond), 110(6): 1263–1270

Pan L, Xiao X, Pan B, Meng C, Staebler R M, Zhang C, Qin Y (2024). Interannual variations and trends of gross primary production and transpiration of four mature deciduous broadleaf forest sites during 2000–2020. Remote Sens Environ, 304: 114042

Pastorello G, Trotta C, Canfora E, Chu H, Christianson D, Cheah Y W, Poindexter C, Chen J, Elbashandy A, Humphrey M, Isaac P, Polidori D, Reichstein M, Ribeca A, van Ingen C, Vuichard N, Zhang L, Amiro B, Ammann C, Arain M A, Ardö J, Arkebauer T, Arndt S K, Arriga N, Aubinet M, Aurela M, Baldocchi D, Barr A, Beamesderfer E, Marchesini L B, Bergeron O, Beringer J, Bernhofer C, Berveiller D, Billesbach D, Black T A, Blanken P D, Bohrer G, Boike J, Bolstad P V, Bonal D, Bonnefond J M, Bowling D R, Bracho R, Brodeur J, Brümmer C, Buchmann N, Burban B, Burns S P, Buysse P, Cale P, Cavagna M, Cellier P, Chen S, Chini I, Christensen T R, Cleverly J, Collalti A, Consalvo C, Cook B D, Cook D, Coursolle C, Cremonese E, Curtis P S, D'Andrea E, da Rocha H, Dai X, Davis K J, Cinti B D, Grandcourt A, Ligne A D, De Oliveira R C, Delpierre N, Desai A R, Di Bella C M, Tommasi P, Dolman H, Domingo F, Dong G, Dore S, Duce P, Dufrêne E, Dunn A, Dušek J, Eamus D, Eichelmann U, ElKhidir H A M, Eugster W, Ewenz C M, Ewers B, Famulari D, Fares S, Feigenwinter I, Feitz A, Fensholt R, Filippa G, Fischer M, Frank J, Galvagno M, Gharun M, Gianelle D, Gielen B, Gioli B, Gitelson A, Goded I, Goeckede M, Goldstein A H, Gough C M, Goulden M L, Graf A, Griebel A, Gruening C, Grünwald T, Hammerle A, Han S, Han X, Hansen B U, Hanson C, Hatakka J, He Y, Hehn M, Heinesch B, Hinko-Najera N, Hörtnagl L, Hutley L, Ibrom A, Ikawa H, Jackowicz-Korczynski M, Janouš D, Jans W, Jassal R, Jiang S, Kato T, Khomik M, Klatt J, Knohl A, Knox S, Kobayashi H, Koerber G, Kolle O, Kosugi Y, Kotani A, Kowalski A, Kruijt B, Kurbatova J, Kutsch W L, Kwon H, Launiainen S, Laurila T, Law B, Leuning R, Li Y, Liddell M, Limousin J M, Lion M, Liska A J, Lohila A, López-Ballesteros A, López-Blanco E, Loubet B, Loustau D, Lucas-Moffat A, Lüers J, Ma S, Macfarlane C, Magliulo V, Maier R, Mammarella I, Manca G, Marcolla B, Margolis H A, Marras S, Massman W, Mastepanov M, Matamala R, Matthes J H, Mazzenga F, McCaughey H, McHugh I, McMillan A M S, Merbold L, Meyer W, Meyers T, Miller S D, Minerbi S, Moderow U, Monson R K, Montagnani L, Moore C E, Moors E, Moreaux V, Moureaux C, Munger J W, Nakai T, Neirynck J, Nesic Z, Nicolini G, Noormets A, Northwood M, Nosetto M, Nouvellon Y, Novick K, Oechel W, Olesen J E, Ourcival J M, Papuga S A, Parmentier F J, Paul-Limoges E, Pavelka M, Peichl M, Pendall E, Phillips R P, Pilegaard K, Pirk N, Posse G, Powell T, Prasse H, Prober S M, Rambal S, Rannik Ü, Raz-Yaseef N, Rebmann C, Reed D, Dios V R, Restrepo-Coupe N, Reverter B R, Roland M, Sabbatini S, Sachs T, Saleska S R, Sánchez-Cañete E P, Sanchez-Mejia Z M, Schmid H P, Schmidt M, Schneider K, Schrader F, Schroder I, Scott R L, Sedlák P, Serrano-Ortíz P, Shao C, Shi P, Shironya I, Siebicke L, Šigut L, Silberstein R, Sirca C, Spano D, Steinbrecher R, Stevens R M, Sturtevant C, Suyker A, Tagesson T, Takanashi S, Tang Y, Tapper N, Thom J, Tomassucci M, Tuovinen J P, Urbanski S, Valentini R, van der Molen M, van Gorsel E, van Huissteden K, Varlagin A, Verfaillie J, Vesala T, Vincke C, Vitale D, Vygodskaya N, Walker J P, Walter-Shea E, Wang H, Weber R, Westermann S, Wille C, Wofsy S, Wohlfahrt G, Wolf S, Woodgate W, Li Y, Zampedri R, Zhang J, Zhou G, Zona D, Agarwal D, Biraud S, Torn M, Papale D (2020). The FLUXNET2015 dataset and the ONEFlux processing pipeline for eddy covariance data. Sci Data, 7(1): 225

Peng S, Piao S, Shen Z, Ciais P, Sun Z, Chen S, Bacour C, Peylin P, Chen A (2013). Precipitation amount, seasonality and frequency regulate carbon cycling of a semi-arid grassland ecosystem in Inner Mongolia, China: a modeling analysis. Agric For Meteorol, 178–179: 46–55

Running S W, Zhao M (2019). Daily GPP and Annual NPP (MOD17A2H/A3H) and Year-end Gap- Filled (MOD17A2HGF/A3HGF) Products NASA Earth Observing System MODIS Land Algorithm (For Collection 6). In: The Numerical Terradynamic Simulation Group, Missoula, MT, USA

Ryu Y, Jiang C, Kobayashi H, Detto M (2018). MODIS-derived global land products of shortwave radiation and diffuse and total photosynthetically active radiation at 5km resolution from 2000. Remote Sens Environ, 204: 812–825

Scott R L, Biederman J A (2017). Partitioning evapotranspiration using long-term carbon dioxide and water vapor fluxes. Geophys Res Lett, 44(13): 6833–6840

Scott R L, Biederman J A, Hamerlynck E P, Barron-Gafford G A (2015). The carbon balance pivot point of southwestern U. S. semiarid ecosystems: insights from the 21st century drought. J Geophys Res Biogeosci, 120(12): 2612–2624

Scott R L, Johnston M R, Knowles J F, MacBean N, Mahmud K, Roby M C, Dannenberg M P (2023). Interannual variability of spring and summer monsoon growing season carbon exchange at a semiarid savanna over nearly two decades. Agric For Meteorol, 339: 109584

Sen P K (1968). Estimates of the regression coefficient based on Kendall's Tau. J Am Stat Assoc, 63(324): 1379–1389

Shen H, Li X, Cheng Q, Zeng C, Yang G, Li H, Zhang L (2015). Missing information reconstruction of remote sensing data: a technical review. IEEE Geosci Remote Sens Mag, 3(3): 61–85

Sjöström M, Zhao M, Archibald S, Arneth A, Cappelaere B, Falk U, de Grandcourt A, Hanan N, Kergoat L, Kutsch W, Merbold L, Mougin E, Nickless A, Nouvellon Y, Scholes R J, Veenendaal E M, Ardö J (2013). Evaluation of MODIS gross primary productivity for Africa using eddy covariance data. Remote Sens Environ, 131: 275–286

Still C J, Berry J A, Collatz G J, DeFries R S (2003). Global

distribution of C3 and C4 vegetation: carbon cycle implications. Global Biogeochemical Cycles 17, 6–1–6–14

Stoy P C, El-Madany T S, Fisher J B, Gentine P, Gerken T, Good S P, Klosterhalfen A, Liu S, Miralles D G, Perez-Priego O, Rigden A J, Skaggs T H, Wohlfahrt G, Anderson R G, Coenders-Gerrits A M J, Jung M, Maes W H, Mammarella I, Mauder M, Migliavacca M, Nelson J A, Poyatos R, Reichstein M, Scott R L, Wolf S (2019). Reviews and syntheses: turning the challenges of partitioning ecosystem evaporation and transpiration into opportunities. Biogeosciences, 16(19): 3747–3775

Swain D L, Langenbrunner B, Neelin J D, Hall A (2018). Increasing precipitation volatility in twenty-first-century California. Nat Clim Chang, 8(5): 427–433

Tucker C J (1979). Red and photographic infrared linear combinations for monitoring vegetation. Remote Sens Environ, 8(2): 127–150

Turner D P, Ritts W D, Cohen W B, Gower S T, Zhao M, Running S W, Wofsy S C, Urbanski S, Dunn A L, Munger J W (2003). Scaling Gross Primary Production (GPP) over boreal and deciduous forest landscapes in support of MODIS GPP product validation. Remote Sens Environ, 88(3): 256–270

Wagle P, Kakani V G (2014). Environmental control of daytime net ecosystem exchange of carbon dioxide in switchgrass. Agric Ecosyst Environ, 186: 170–177

Wagle P, Xiao X, Scott R L, Kolb T E, Cook D R, Brunsell N, Baldocchi D D, Basara J, Matamala R, Zhou Y, Bajgain R (2015a). Biophysical controls on carbon and water vapor fluxes across a grassland climatic gradient in the United States. Agric For Meteorol, 214–215: 293–305

Wagle P, Xiao X, Suyker A E (2015b). Estimation and analysis of gross primary production of soybean under various management practices and drought conditions. ISPRS J Photogramm Remote Sens, 99: 70–83

Wagle P, Xiao X, Torn M S, Cook D R, Matamala R, Fischer M L, Jin C, Dong J, Biradar C (2014). Sensitivity of vegetation indices and gross primary production of tallgrass prairie to severe drought. Remote Sens Environ, 152: 1–14

Wang X, Xiao X, Zou Z, Chen B, Ma J, Dong J, Doughty R B, Zhong Q, Qin Y, Dai S, Li X, Zhao B, Li B (2020). Tracking annual changes of coastal tidal flats in China during 1986–2016 through analyses of Landsat images with Google Earth Engine. Remote Sens Environ, 238: 110987

Winslow J C, Hunt E R Jr, Piper S C (2003). The influence of seasonal water availability on global C3 versus C4 grassland biomass and its implications for climate change research. Ecol Modell, 163(1−2): 153–173

Xiao X (2006). Light absorption by leaf chlorophyll and maximum light use efficiency. IEEE Trans Geosci Remote Sens, 44(7): 1933–1935

Xiao X, Biradar C M, Czarnecki C, Alabi T, Keller M (2009). A simple algorithm for large-scale mapping of evergreen forests in tropical America, Africa and Asia. Remote Sens (Basel), 1(3): 355–374

Xiao X, Hollinger D, Aber J, Goltz M, Davidson E A, Zhang Q, Moore B III (2004a). Satellite-based modeling of gross primary production in an evergreen needleleaf forest. Remote Sens Environ, 89(4): 519–534

Xiao X, Zhang Q, Braswell B, Urbanski S, Boles S, Wofsy S, Moore B, Ojima D (2004b). Modeling gross primary production of temperate deciduous broadleaf forest using satellite images and climate data. Remote Sens Environ, 91(2): 256–270

Xin F, Xiao X, Zhao B, Miyata A, Baldocchi D, Knox S, Kang M, Shim K, Min S, Chen B, Li X, Wang J, Dong J, Biradar C (2017). Modeling gross primary production of paddy rice cropland through analyses of data from CO_2 eddy flux tower sites and MODIS images. Remote Sens Environ, 190: 42–55

Xu L, Baldocchi D D (2004). Seasonal variation in carbon dioxide exchange over a Mediterranean annual grassland in California. Agric For Meteorol, 123(1−2): 79–96

Yan H, Fu Y, Xiao X, Huang H Q, He H, Ediger L (2009). Modeling gross primary productivity for winter wheat–maize double cropping system using MODIS time series and CO_2 eddy flux tower data. Agric Ecosyst Environ, 129(4): 391–400

Zhang Y, Xiao X, Wu X, Zhou S, Zhang G, Qin Y, Dong J (2017). A global moderate resolution dataset of gross primary production of vegetation for 2000–2016. Sci Data, 4(1): 170165

Zhao M, Heinsch F A, Nemani R R, Running S W (2005). Improvements of the MODIS terrestrial gross and net primary production global data set. Remote Sens Environ, 95(2): 164–176

Zheng Y, Shen R, Wang Y, Li X, Liu S, Liang S, Chen J M, Ju W, Zhang L, Yuan W (2020). Improved estimate of global gross primary production for reproducing its long-term variation, 1982–2017. Earth Syst Sci Data, 12(4): 2725–2746

Zhou S, Yu B, Zhang Y, Huang Y, Wang G (2016). Partitioning evapotranspiration based on the concept of underlying water use efficiency. Water Resour Res, 52(2): 1160–1175

Zhu X, Pei Y, Zheng Z, Dong J, Zhang Y, Wang J, Chen L, Doughty R B, Zhang G, Xiao X (2018). Underestimates of grassland gross primary production in MODIS standard products. Remote Sens (Basel), 10(11): 1771